DOI: 10.15480/882.9319

Eighth International Symposium on Marine Propulsors
smp'24, Berlin, Germany, March 2024

Influence of Head Waves Encounter on the KRISO Container Ship (KCS) Propulsion

Hisham Gamal[1], Mohammed Abbas Kotb[2], Moustafa Abdel-Maksoud[3], Tamer Mahmoud Ahmed[2]

[1]Egyptian Naval Forces, Alexandria, Egypt
[2]Alexandria University, Alexandria, Egypt
[3]Hamburg University of Technology (TUHH), Hamburg, Germany

ABSTRACT

The hull-propeller interaction has a significant impact on the propulsion performance of ships. The interaction parameters are mostly investigated under the assumption of calm water conditions, although in real operation, the influence of the waves and ship motion may be significant. The aim of the study is to determine the influence of head-waves on the interaction between the hull, the propeller, and the rudder as well as on the overall propulsive efficiency. In this numerical study, the viscous flow on the KRISO Container ship (KCS) model is calculated in calm water and in head-waves. The required power and propeller performance are estimated at different steepnesses of the incoming waves. The RANS code STAR-CCM+ is applied to evaluate the propulsion performance of the KCS fitted with the KP505 propeller in model scale. A PID controller is applied to keep the ship speed constant in calm water and in waves.

The propeller flow is simulated using two approaches, namely, the virtual actuator disk (AD) and the discretized propeller (DP). The numerical setup is validated using published data for propulsion tests at different speeds.

The obtained results show that the wave-induced velocity components change the wake field significantly. The increase in the wave steepness leads to a strong fluctuation in the wake velocity field and the required thrust as well as to higher power losses Furthermore, the results obtained confirm that the presence of the rudder behind the propeller leads to an improvement in propulsion efficiency not only in calm water but also in waves.

Keywords

Propulsion; Added Power; Resistance; Wave Steepness; Head waves.

1 INTRODUCTION

The computation of added power due to ship motion in waves is always a challenge. Therefore, there is a high demand for the development of methods to predict the effects of the waves on the propeller efficiency and the required power with the desired accuracy. A comprehensive quantification of the effects of the waves on the propeller performance must include the analysis of the nominal wake field and the effective wake field. In addition, the rudder and its position can also affect the performance of the propeller and the added power as well.

Different experimental studies are conducted to investigate the ship's propulsive performance, (Øyan 2012) and (Kayano et al 2013). In these experiments, the load-varying self-propulsion approach was used to estimate ship speed and power demand.

At present, computational fluid dynamics (CFD) has become a powerful option for carrying out extensive hydrodynamic analyses. RANS solvers are widely employed for investigating maneuvering and seakeeping problems (Kim 2019). A considerable number of numerical investigations of the viscous flow on the KCS hull geometry has been conducted in the last years, (Carrica et al. 2011), (Soe et al 2017), (Simonsen et al 2014), (Sadat-Hosseini et al 2015), (Kim 2017) , (Hao & Wan, 2019), (Hafizul & Doares 2021). CFD Ship-Iowa code was utilized to simulate the flow on a self-propelled model using the Body Force method (BF) based on the blade element theory, (Simonsen et al 2013). The comparison with the experimental data shows a good agreement for the global and local flow quantities in calm water and in head waves.

In the present study, the ship propulsion characteristics of the KCS model are investigated in head waves. The added power and the wake field in waves is studied at different steepness using STAR-CCM+.

1.1 Hull, Propeller, and Rudder

The local coordinate system of the ship matches the global coordinate system as reflected in Figure 1. The origin is located at the ship's center of mass.

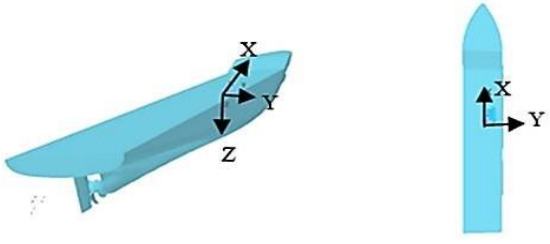

Figure 1: Ship local coordinate system.

Table (1) illustrates the main hull parameters in full and model scale. In the presented work, all simulations are performed in ship model scale of the MOERI model.

Table 1: KCS main particulars.

	Full scale	Model scale
Scale	1.000	31.599
Lpp (m)	230.0	7.2786
Lwl (m)	232.5	7.3570
Bwl (m)	32.2	1.0190
D (m)	19.0	0.6013
T (m)	10.8	0.3418
Displacement (m^3)	52030	1.6490
S w/o rudder (m^2)	9530	9.5441
S (m^2) incl. rudder	9645	9.659
LCG (m)	111.6	3.532
GM (m)	0.60	0.019
Ixx/B	0.40	0.40
Izz/Lpp	0.25	0.25

Figure 2 shows the positive direction of the propeller rotation axis which is in the direction of the ship's longitudinal axis.

Figure 2: Propeller local coordinate system.

Figure 3 shows the results of the open water test of KP505 presented in SIMMAN 2008, (Stern et al 2008). The experimental results are used as input data in the setup of the actuator disk.

.

Whereas:

k_T: Thrust coefficient.

k_Q: Torque coefficient

η_0: Propeller open water efficiency.

J: Flow advance ratio.

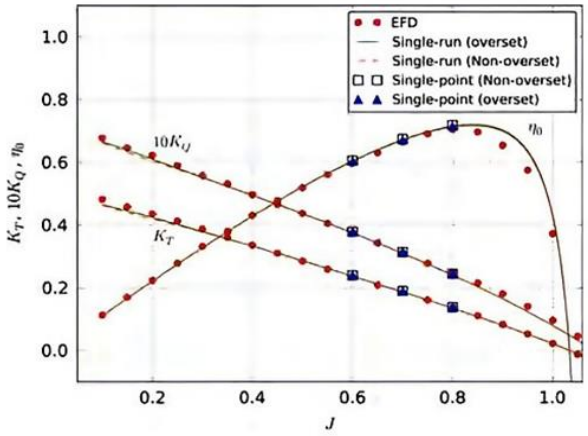

Source: KCS Geometry and Conditions, SIMMAN 2008

Figure3: Propeller open water test data.

The main parameters of the kp505 propeller in full scale are as follows: diameter is 7.9 m and hub ratio is 0.18. The propeller is a right-handed propeller. The pitch diameter ratio is 0.997. The propeller is a fixed pitch propeller with expanded area ratio (A_e/A_o) of 0.8.

2 METHODOLOGY

The numerical computations are conducted using the RANS solver STAR-CCM+. A verification and validation (V&V) study is performed to evaluate the performance of the numerical setup developed in the presented work. The experimental data published in the Workshop on CFD in Ship Hydrodynamics and Simulation Methods (Larsson et al. 2015) as well as those recently presented by Guo & Wan (2019) and Islam & Soares (2021) are used for the comparison.

2.1 Governing Equations

The governing equations that describe the fluid flow are the continuity equation that represents the mass conservation and the momentum conservation equation, see Equations (1).

$$\frac{\partial}{\partial t}\int_{\Omega} \rho \, d\Omega + \int_{S} \rho \vec{v}.\vec{n} \, dS = 0 \qquad (1)$$

Equation (2) represents Newton's second law as the rate of change of the momentum equal to the forces applied on the fluid.

$$\frac{\partial}{\partial t}\int_{\Omega} \rho \vec{v} \, d\Omega + \int_{S} \rho \vec{v}\vec{v}.\vec{n} \, dS = \int_{S} Tw \, dS + \int_{\Omega} \rho b \, d\Omega \qquad (2)$$

As ρ: fluid density, t: time.

Ω: control volume that contains the control mass.

$\vec{v}$: the fluid velocity vector, $\vec{n}$: unit vector normal to the control surface area.

S: control surface area, T: Stress tensor.

μ: Fluid viscosity, b : body force

2.2 Domain Boundaries

In both cases, i.e. calm water and regular head waves, the inflow is assumed to move in the opposite direction to the surge motion of the ship, at an encounter angle of 180 degrees, as shown in Figure (4). This corresponds to the propagation direction of the wave, the wind and the current.

The upper boundary is defined as a pressure outlet and the lower boundary as a slip wall. All other boundaries: left, right, inlet and outlet are defined as velocity inlet; thus, the flow velocities at these boundaries are needed in the equations used in field functions defining the forcing zones. This technique is applied to minimize wave reflection at the boundaries by introducing source term in the momentum equation to damp the reflected.

The velocities of the flow at these boundaries are updated during simulations using embedded field functions that read the velocity of the flow in both cases of a fifth order

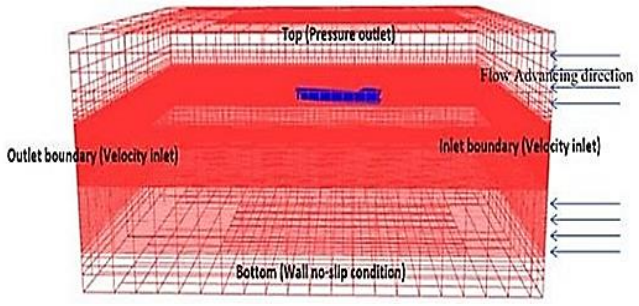

Figure4: Domain boundaries.

2.3 Boundary Layer and Turbulent Model

An accurate prediction of the flow in the wall near regions is important to achieve realistic results of the flow field on the ship and the propeller inflow. In addition to the choice of the turbulence model, the realization of a high grid resolution in the boundary layer region is important in order to improve the quality of the simulation results. Therefore, the boundary layer is discretized using prism layer grid, which is defined based on the boundary layer thickness, the number of layers and the stretching factor. The commonly used turbulent model $k-\omega$ SST is applied in the present study.

2.4 Effect of Waves Reflection on the Results

Previous investigations and studies confirm that the wave reflected from domain boundaries can introduce significant errors, (Peric, 2019). Therefore, minimizing these reflections at the domain boundaries is very important to ensure the quality of the simulation results. The parameter that can measure the reflection intensity is the reflection coefficient CR. The reflection coefficient CR can be defined as a ratio between the reflected wave height (amplitude) to the generated wave height (amplitude) by the ship. See Equations (3) and (4) (Peric, 2019).

$$CR = \frac{H_{Refl}}{H_{gen}} \quad or \quad C_R^2 = \frac{E_{Refl}}{E_{gen}} \quad \text{for free surface waves} \qquad (3)$$

$$CR = \frac{a_{Refl}}{a_{gen}} \qquad for\ harmonic\ waves \qquad (4)$$

2.5 Forcing Zones

There are different methods to minimize the wave reflection at the domain boundaries. In the case of free surface simulations, the reflection coefficient must not exceed 0.1, and by applying the method developed by Perić & Abdel-Maksoud (2018) it can be kept in the range of 0.01 to 0.02. In the presented study, forcing zones method is applied to damp waves at the domain boundaries.

Two parameters must be selected to define the forcing zone; the thickness of the forcing zone (x_d) and the strength of the source term added in the governing equation (γ).

These parameters depend on specifications of the wave characteristics such angular frequency and length. In addition, the resolution of numerical grid and the local variation of cell size can also influence the reflection coefficient values. The strength factor γ is proportional to the wave angular frequency and inversely proportional to the wavelength (Peric, 2019). The forcing zone thickness is directly proportional to the wavelength.

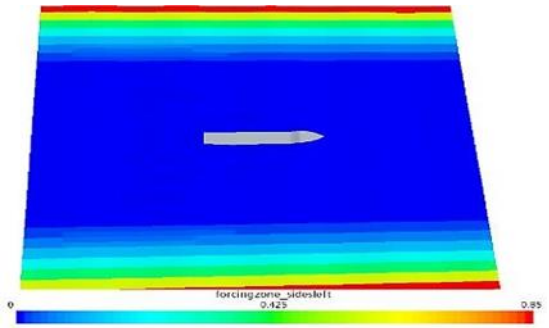

Figure5: Forcing zones at boundaries.

2.6 Numerical Grids

The grid used in the current simulations is optimized to minimize the number of cells by coursing the background and increasing the resolution gradually by a custom volume mesh. For the grid convergence and according to the ITTC guidelines, four different mesh sizes are used in the convergence study and the overlapping mesh was utilized as interface between the background and the dynamic domain, (ITTC 2014). In the case of the self-propelled model with the discretized propeller DP, the overset mesh was used as an interface between the propeller and the overset domain of the ship.

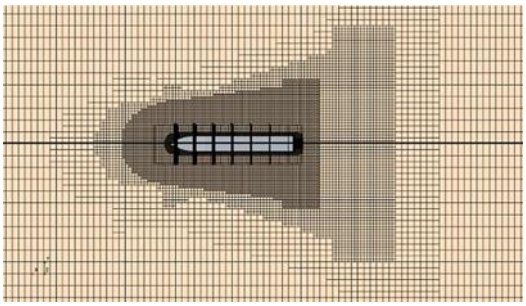

Figure6:Numerical grid.

2.6.1 Grid Used in the Overset Domain

For the overset domain (ship dynamic domain), four mesh sizes were used in the convergence study, see Table 2. The overlapping grid approach preserves the benefits of structured grids while offering the flexibility of unstructured grids. Even though all component grids in ship flow are structured, overlapping grids provide the additional benefit of not relying on the usage of structured grid configurations.

Table 2: Number of cells used in each simulation.

Case	Number of cells
Half of the domain only	550,000
Full domain with AP	3,150,000
Half of the domain with VD	1,200,000
Full domain with VD	2,400,000

2.6.2 Grid Used in the Discretized Propeller

The mesh used for the propeller discretization is shown in Figure 7. The overset mesh approach is applied to create the interface between the propeller and the background of the hull.

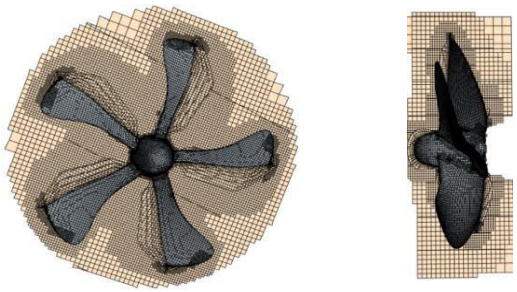

Figure7: Propeller meshing.

2.7 Test Cases

The computations are carried out for Froude number 0.26 in calm water and head waves with a wave length equal to the ship length. As mentioned above, 3 wave steepness are considered in the simulations, namely 1/60, 1/50, and 1/40. The waves are generated using the 5th order Stokes theory. All simulations for the self-propulsion tests are carried out using virtual disc and real propeller geometry.

2.8 Numerical Probes

The numerical probes used to measure the inflow velocities beyond the propeller plane are illustrated in Figure 8. The angle between the probes is 5 degrees step in the radial direction. Eleven radii are considered starting from 0.18 r/R to 1.1 r/R. The location of the probes is at a distance of 0.4D (propeller diameter) in the front of the leading edge of the propeller. The relative velocity between the probe and the inflow is taken into account as the probes are moving with the ship's hull speed.

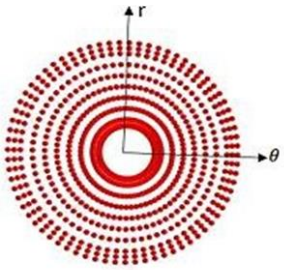

Figure8: Numerical probes.

2.9 Physical Time Step and Courant Number

The Courant-Friedrichs-Lewy (CFL) condition states that; any information passing through the mesh during the time step length must travel a shorter distance than the space between the mesh elements. In other words, information from a specific cell or mesh element must only reach its close neighbor elements. The Courant number formula (5) is derived from the CFL condition and is as follows according to Hino et al. (2021):

Where, c is the Courant number, u is the velocity magnitude, Δt is the time step size and, Δx is the length of the mesh elements. c must be less than 1, ideally less than 0.7. The particle "skips" a cell if the Courant number is greater than 1, meaning that; the time step is too large to notice the particle in that cell. The particle remains in the cell for at least two-time steps if it is less than 0.7. Once the Courant number is greater than 1, instabilities can be magnified across the entire domain and may result in simulation divergence. As a result, there are two options for lowering the Courant number, namely:

• Decrease the time step Δt.

•Coarsen the mesh i.e., increase the size of the mesh elements.

$$C = \frac{u\Delta t}{\Delta x} \qquad (5)$$

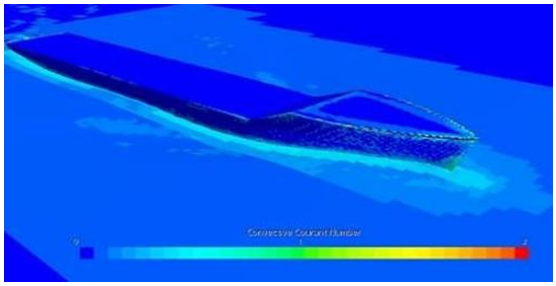

Figure 9: Courant number.

3 RESULTS

Results of the simulations with regards to propulsion performance (torque, number of revolutions and delivered power) are presented and analyzed for calm water as well as in head waves with different steepness ratios.

3.1 Added Power Results

In this section, results of the added power from different simulations are illustrated and compared. The section starts with results of the simulations performed using the virtual disk VD of the still water case and the three simulations with wave steepness of 1/60, 1/50, and 1/40 respectively. Afterwards, the corresponding results for the simulations with discretized propellers are presented.

The wake field results are illustrated and compared in the same manner.

3.1.1 Virtual Disc (VD) Results

Results of the simulations using the VD are described and discussed in terms of the propeller's required number of revolutions per second and in terms of the dimensionless coefficients such as, the thrust and torque coefficients and the advance speed ratio. In addition, the estimated efficiencies of the propeller behind the ship, the delivered power and the relative rotation efficiencies are all illustrated as well. Table 3 shows the results from VD simulations. Cases 0,1,2 and 3 represent calm water, head waves with steepness of 1/60, 1/50 and 1/40 respectively.

Table 3: Results of VD simulations.

Case	*0*	*1*	*2*	*3*
n (rps)	9.35	12.48	13.59	15.125
n'= n LBP/ V	30.82	40.92	44.557	49.08
kT	0.183	0.248	0.26	0.272
10 kQ	.300	0.380	0.420	0.440
J	0.7	0.566	0.539	0.5
ηRR	1.005	0.78	0.694	0.6
ηB	0.665	0.518	0.461	0.4
Delivered power. kw	0.157	0.446	0.702	0.895
Thrust power. kw	0.104	0.227	0.354	0.456

3.1.2 Discretized Propeller (DP) Results

The utilization of VD allows significant reductions in time and computational effort and keeps the number of cells used to a minimum. VD models are efficient especially for estimation the required propulsion power. Results of the actual discretized propeller are illustrated in the same manner in Table 4. As it may be seen, the calculated thrust and torque coefficients in waves are much higher than in calm water. The computed thrust and torque coefficients for the different wave steepnesses do not show clear correlations, but when the delivered power is considered, a considerable increase in the power requirement is visible when the waves become steeper.

Finally, a comparison between VD and DP is illustrated in Figure 10 in terms of number of revolutions, thrust and torque coefficients, quasi-propulsive efficiency, delivered power and thrust power.

Table 4: Results of DP simulations.

Case	0	1	*2*	*3*
n'= n LBP/ V	30.82	40.92	44.55	49.08
kT	0.17	0.23	0.22	0.21
kQ	0.02	0.04	0.03	0.03
J	0.65	0.57	0.55	0.54
ηRR	1.00	0.78	0.69	0.6
ηB	0.64	0.54	0.53	0.5
Delivered power. kw	0.15	0.59	0.75	0.83
Thrust power kw	0.108	0.30	0.37	0.49

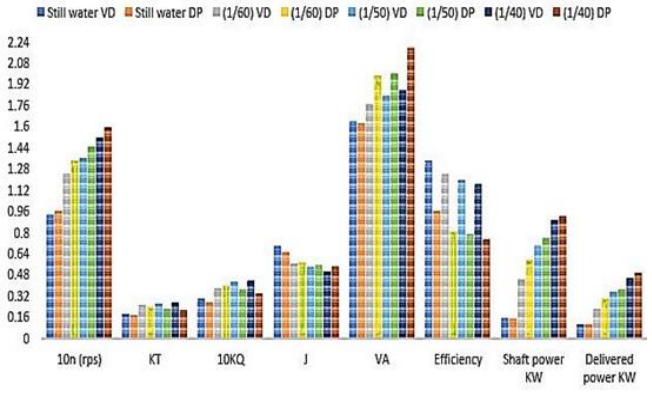

Figure 10: Results in waves of VD and DP.

3.2 Results of Wake Field Distribution

In this section, results of the wake field of simulations conducted are illustrated and discussed. It starts with the wake distribution in still water and ends with results of the simulations for different wave steepness. Results of different wave steepness are illustrated in terms of wake fraction contours followed by analysis.

3.2.1 Wake Field Results in Calm Water

The advance speed of the flow is one of the most critical parameters that can have a strong influence on the performance of the propeller behind the ship, (Wu et al 2016). The propeller inflow is characterized by the hull form, the radial thrust distribution of the propeller, and the interaction with the rudder.

Figure 11 illustrates four different cases of the wake fraction distribution. These cases are the nominal wake fraction without the propeller but with the rudder, the virtual disk with and without the rudder and finally, the case of the existence of the discretized propeller and the rudder. As expected, the results show that the existence of the propeller in both cases, with or without the rudder, decreases the wake fraction contours but, this decrease is particularly significant in the case of propeller and rudder existence since, the interaction between the propeller and the rudder increases the induced velocity at the propeller plane due to the reduction of the swirl losses in the propeller slipstream.

The results are presented at two locations, one at 10% of the propeller radius at 0.0125 m in the front of the propeller leading edge and the second location at 0.1m in the front of the propeller.

The rudder converts a part of the swirl energy of the flow in the propeller slipstream into axial velocity component and therefore, the axial flow velocity behind it increases, (Naz 2019). Due to the propeller impact on the inflow and the interaction between the propeller and the rudder, an accelerated axial flow component is induced far in front of the propeller, and continues a certain distance behind the rudder.

Figure 11 shows that at a distance of 0.1 m from the propeller, the velocity distribution calculated with VD and DP are in good agreement. In contrast, the flow calculated with VD at a distance of 0.0125 m from the propeller is greatly accelerated compared to the results obtained with DP. The reason for this is that with VD the influence of the source terms is locally very strong and this leads to a local acceleration of the flow, this occurs particularly when the defined thickness of the virtual disc is small.

3.2.2 Wake Field Results in Waves

The investigation of the wake field behind the hull is very complicated in waves as, the wake distribution changes with the ship's motions, Figure 12 and Figure 13 show results of the wake fraction contours in waves with different wave steepness using VD and DP. The results of the measuring plane at the location of 0.0125m are presented for each wave steepness; once, for the case of a wave crest amidships and, once for the case of a wave

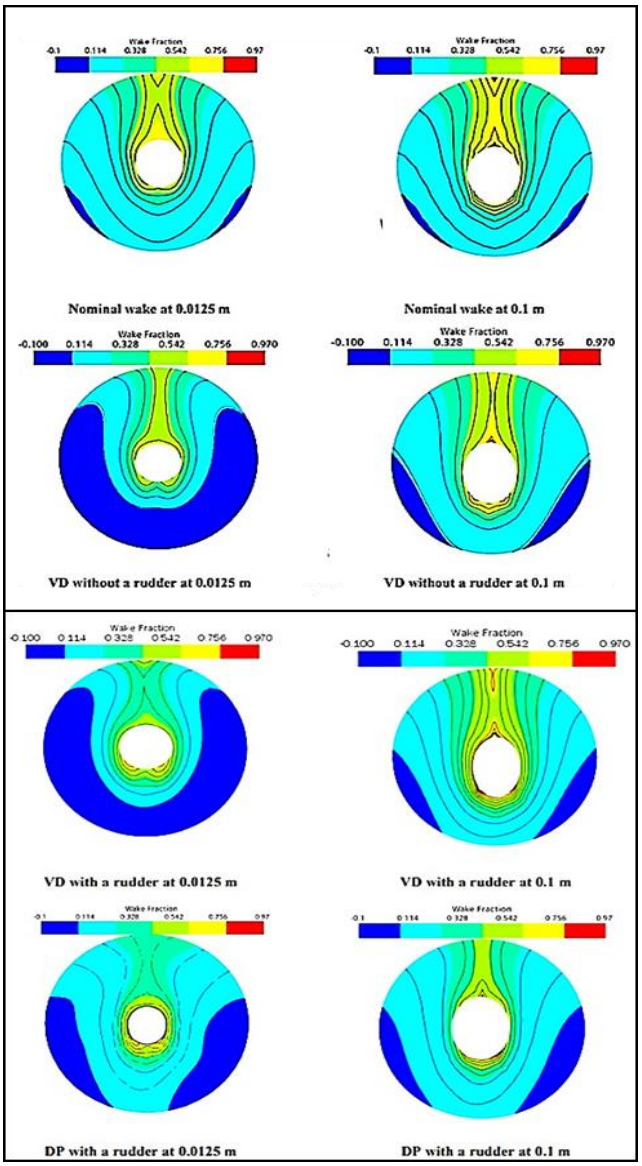

Figure 11: VD and DP results in still water.

trough amidships. The wave applied in the simulations has an encounter frequency close to the resonance frequency of ship pitch motion. As a result, there is a phase shift of 90 degrees between the wave motion and the ship motion.

The pitch motion changes the orientation of the ship's hull and the inflow angle as well. Results show that as the steepness wave increases, the wake fraction is reduced. When the wave trough is amidships, the wake fraction is less than the case of a wave crest amidships. When the wave crest amidships, the ship will have a positive pitch motion (stern is moving downwards), the axial component of advance speed (Va) decreases and the wake fraction increased. When the wave trough amidships, the ship will have a negative pitch motion (bow is moving downwards), the axial component of the advance speed of the inflow increases, which decreases the wake fraction coefficient.

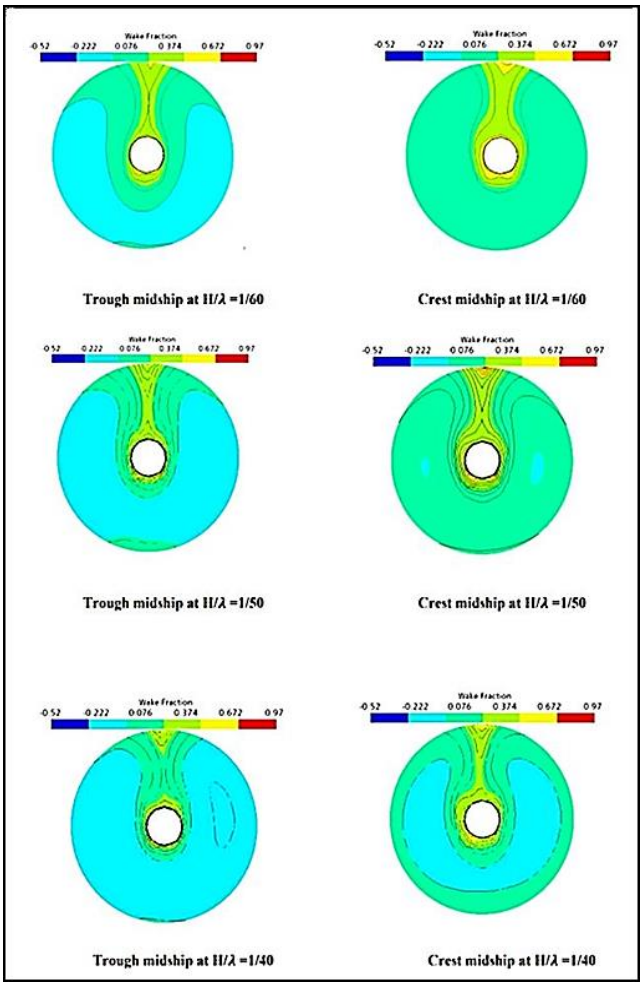

Figure 12: Wake fraction results in waves using VD.

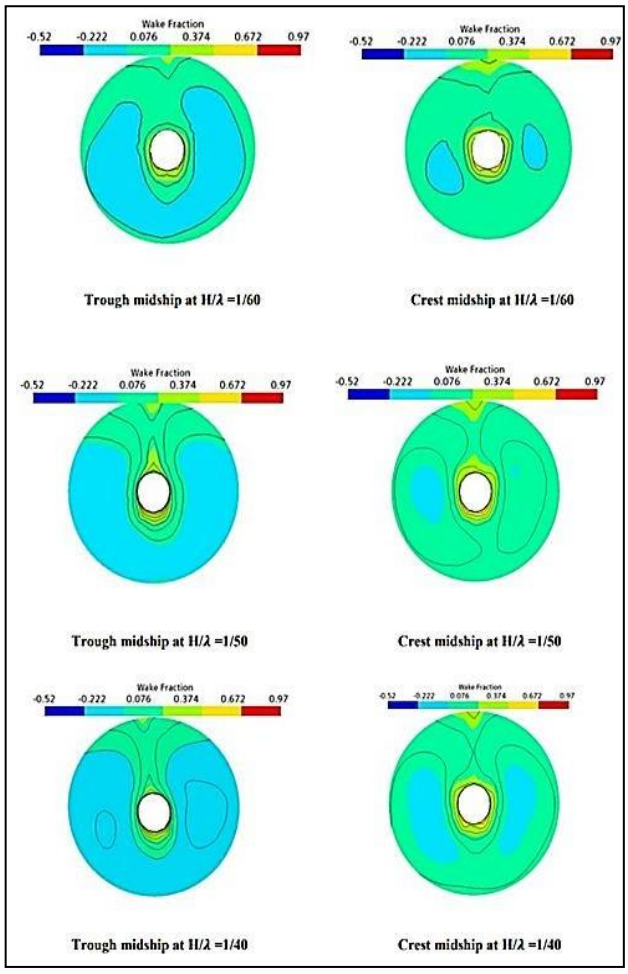

Figure 13: Wake fraction results in waves using DP.

4 Conclusions

The results show that the power demand increases considerably with increasing the wave steepness. At high wave steepness, the induced particle velocity influences the wake field in a significant manner. Waves drastically reduce the efficiency of the propeller due to the increase in the thrust loading coefficient. The increase in wave steepness leads to a strong fluctuation in the wake velocity and the required thrust as well. Consequently, this causes an additional decrease in the propeller efficiency.

Presence of the rudder leads to a modification of the velocity field in the propeller plane and the propeller slipstream, resulting in an increase in the propeller thrust and consequently improves the propeller efficiency in behind condition compared with the open water test.

ACKNOWLEDGEMENTS

The authors are very grateful to Mr. Jannes Berndt, Hamburg University of Technology Centrale de Nantes, France, for his helpful suggestions in the numerical simulations' setup. Additionally, special gratitude thanks to the Maritime Technology Studies Institute (MTSI) for providing their facilities and servers to conduct the simulations and the academic work.

REFERENCES

Carrica, P.M., Fu, H. & Stern, F. (2011) 'Computations of self-propulsion free to sink and trim and of motions in head waves of the KRISO container ship (KCS) model.'Applied Ocean Research.

Hao, G., & Wan, D. (2019). 'Study of wave added resistance and motions of KCS in waves with different wave lengths'. Proceedings of the ASME 2019 38th International Conference on Ocean, Offshore and Arctic Engineering, OMAE2019-95526, Glasgow, Scotland, UK.

Hino, T., Stern, F., Larsson, L., Visonneau, M., Hirata, N., & Kim, J. (2021). Lecture Notes in Applied and Computational Mechanics 94.

Hafizul, I., & Soares, C. G. (2021). 'Head Wave Simulation of a KCS Model Using Open foam for the Assessment of Sea-Margin'. International Conference on Offshore Mechanics and Arctic Engineering - OMAE 8 (June).

ITTC. (2014). Practical Guidelines for Ship CFD Applications. ITTC – Recommended Procedures and Guidelines ITTC, 1–8.

Kayano, J., Hideo, Y., Sasaki, N.i & Hiwatashi, R. (2013). 'A study on the propulsion performance in the actual

sea by means of Full-Scale Experiments'. TransNav, the International Journal on Marine Navigation and Safety of Sea Transportation.

Kim, M., Hizir, O., Turan, O. & Incecik, A. (2017). 'Numerical studies on added-resistance and motions of KVLCC2 in head seas for various ship speeds'. Ocean Engineering, Volume 140.

Kim, D. (2019). 'URANS V & V for KCS free running course keeping and maneuvering simulations in calm water and regular head / oblique waves'. PhD Thesis, University of Iowa.

Larsson, L., Stern, F., Visonneau, M., Hino, T., Nobuyuki Hirata, N. & Kim. J. (2015) 'Proceedings, Tokyo 2015 Workshop on CFD in Ship Hydrodynamics'.

Naz, N. (2019). 'Numerical simulation of flow around ship hull considering rudder-propeller interaction', PhD Thesis, Bangladesh University of Engineering and Technology

Peric, R. (2019). 'Minimizing Undesired Wave Reflection at the Domain Boundaries in Flow Simulations with Forcing Zones'. PhD Thesis Hamburg University of Technology

Perić, R. & Abdel-Maksoud. M. (2018). 'Analytical Prediction of Reflection Coefficients for Wave Absorbing Layers in Flow Simulations of Regular Free-Surface Waves'. Ocean Engineering 147: 132–47.

Øyan, E. 2012. 'Speed and Powering Prediction for Ships Based on Model Testing', Master Thesis, Norwegian University of Science and Technology

Sadat-Hosseini, H., Toxopeus, S., Kim, D. & Castiglione, T. (2015). 'Experiments and Computations for KCS Added Resistance for Variable Heading'. 5th World Maritime Technology Conference, Rhode Island, USA.

Seo, S., Park, S. & Koo, B. (2017). 'Effect of Wave Periods on Added Resistance and Motions of a Ship in Head Sea Simulations'. Ocean Engineering 137.

Simonsen, C., Otzen, J.& Stern, F. 2013. "EFD and CFD for KCS Heaving and Pitching in Regular Head Waves." Journal of Marine Science and Technology.

Simonsen, C., Otzen, J.F., Nielsen, C. & Stern, F. (2014). 'CFD Prediction of Added Resistance of the KCS in Regular Head and Oblique Waves'. *30th Symposium on Naval Hydrodynamics*, Hobart, Tasmania, Australia.

Stern, F. & Agdrup, K. (Ed.) (2008). SIMMAN 2008. 'Workshop on Verification and Validation of Ship Manoeuvring Simulation Methods'. Copenhagen, workshop proceedings: volume 1. Summary, test cases, methods and papers. Force Technology: Brøndby.

Wu, P., Sadat-Hosseini, H., Stern, F. & Toda, Y. (2016). 'Nominal Wake Fluctuation'. Journal of the Japan Society of Naval Architects and Ocean Engineers, March 2016.